ORIGINAL PAPER - PRODUCTION ENGINEERING

Research and application of acid fracturing stimulation mechanism in ultra-deep subsalt dolomite reservoir in Tarim Basin

Jiangyu Liu[1] · Jinming Zhao[2] · Shiyong Qin[1] · Nanlin Zhang[2,3] · Dengfeng Ren[1] · Zhifeng Luo[2] · Yaozeng Xie[2]

Abstract

Deep and ultra-deep carbonate reservoirs are the focus of exploration and development in future. However, the problems of high pressures in the treatment process, a limited effective etching distance of acid, great acid leak-off, and poor adaptability of the acid system are encountered in this type of oil and gas reservoir. The mechanism of acid fracturing stimulation under different processes and parameters is not clear. Aiming at these issues, the treatment schemes, process optimization, parameter optimization, and liquid system screening are studied in this paper, try to clarify the acid fracturing stimulation mechanism, and the following conclusions are drawn: The acid network fracturing could activate natural fracture to generate a complex fracture network to the greatest extent, and thereby a high output could be achieved; By using of weighted fracturing fluid, the wellhead injection pressure, as well as the performance of equipment required, could be effectively reduced; With 20% gelling acid and 20% retarded acid system, the non-uniform etching could be realized to improve the effective etching distance of acid liquid. The conclusions in this paper shed light on the acid fracturing treatment of deep and ultra-deep carbonate rocks.

Keywords Ultra-deep · Subsalt dolomite reservoir · Acid fracturing · Stimulation mechanism · Technology and parameter optimization

List of Symbols

C_f	The hydraulic fracture compression coefficient (MPa^{-1})
C_L	The compressibility coefficient of fluid (MPa^{-1})
C_m	The comprehensive compressibility coefficient of the matrix (MPa^{-1})
C_n	The compression coefficient of natural fracture (MPa^{-1})
K_f	The hydraulic fracture permeability (D)
K_m	The permeability of bedrock (D)
K_n	The natural fracture permeability (D)
L_m	The matrix rock block size (m)
P_f	The pressure of hydraulic fracture system (MPa)
p_{junc}	The intersection pressure (MPa)
P_m	The pressure of bedrock pore system (MPa)
P_n	The pressure of the natural fracture system (MPa)
p_{net}	The net pressure in the fracture (MPa)
p_{tip}	The fluid pressure at the tip of the natural fracture (MPa)
q_f	The volumetric flow rate of liquid at the source divided by that at the sink per unit hydraulic fracture pore volume (s^{-1})
q_n	The volumetric flow rate of liquid at the source divided by that at the sink per unit natural fracture pore volume (s^{-1})
x_o	The distance between the restart and intersection points (m)
α	The matrix shape factor ($12/L_m^2$)
$\delta(M - M')$	Is the delta function, of which the value equals 0 when $M = M'$
Δp_{nf}	The pressure loss in the direction of the natural fracture (MPa)

✉ Nanlin Zhang
  nanlin_zhang@163.com

1. Petrochina Tarim Oilfield Company, Korla 841000, Xinjiang, China

2. State Key Laboratory of Oil and Gas Reservoir Geology and Exploitation, Southwest Petroleum University, Chengdu 610500, Sichuan, China

3. Department of Chemical and Petroleum Engineering, University of Calgary, Calgary, AB T2N 1N4, Canada

Δp_{open}	The pressure loss in the direction of the length of activated natural fracture l (MPa)
Δp_{shear}	The pressure loss in the direction of shear natural fracture length a (MPa)
μ	The fluid viscosity (MPa s)
σ_{hmin} and σ_{Hmax}	The min and max far-field stress (MPa)
σ_{n}	Normal stress (MPa)
τ_0	The shear strength of the natural fracture (MPa)
τ	Tangential stress (MPa)
ϕ_{f}	The porosity of natural fracture (dimensionless)
ϕ_{m}	The matrix porosity (dimensionless)
ϕ_{n}	The porosity of natural fracture (dimensionless)
χ	The starting pressure gradient of bedrock (MPa m^{-1})

Introduction

In the Tarim oilfield, 23 subset ultra-deep dolomite wells have been exploited, and seven-time treatment measures have been implemented in 6 of these wells (Table 1). The acid fracturing process primarily applies to the reservoirs with acid corrosion rates higher than 90%; Sand fracturing technology is principally adopted for reservoirs with low acid corrosion rates or containing gypsum; Generally speaking, currently, the treatment technologies of subsalt ultra-deep dolomite reservoirs do not match with the real situations, and the treatment performance is not good enough. The effective exploitation of subsalt ultra-deep dolomite reservoir is of great importance for the high stable output of the Tarim oilfield.

Research on dolomite reservoir treatment has been reported. Yan carried out acid-rock reaction kinetics experiments with carbonate rock cores containing different dolomite mass fractions (Yan et al. 2021b). The difference in acid corrosion mechanisms of limestone and dolomite was analyzed with the scanning electron microscope, and the models of dolomite acid-rock reaction kinetics determined by different factors were established. Dong et al. (2021) constructed a three-dimensional acid migration model to calculate the geometry of the fracture in acid fracturing treatment. Acid flow, reaction migration, and rock corrosion in fracture were taken into account in this model. The influence of dolomite heterogeneity of the acid corrosion process was analyzed, and the acid corrosion modes in carbonate reservoirs with different spatial distributions of calcite and dolomite minerals were compared. Nino-Penaloza conducted acid-injecting tests on fractured cores of the chalk rock strata in Austin and dolomite strata in San Andres to probe the effects of injection temperature, pumping time, and acid type on the conductivity of fracture. And, the influence of core fracture surface texture before acid injection was investigated with rough and smooth surface textures as the research objects for quantification (Nino-Penaloza et al. 2015). Qi recommended that the user of retarded acid hardly led to high conductivity in the acid fracturing of the dolomite reservoir (Qi et al. 2021). Therefore, according to the acid-etching morphology of fractures, the influencing factors and improvement methods of fracture conductivity were discussed. It was suggested that the etching morphology was not directly related to the determining mechanism of the acid-rock reaction, but dependent on the reaction rate. The reason for low conductivity was the slow reaction between dolomite and retarded acid and the difficult formation of irregular etching grooves on the fracture surface. A small amount of dolomite in the reservoir did not affect the conductivity, but > 80%

Table 1 Seven times treatment measures of 6 wells

Well no.	Number of natural fractures	Lithology	Treatment measures	Effect of stimulation
1.	2	Dolomite containing calcium sulfate	Acid fracturing	Daily oil production 12.5 m^3, daily gas production 5436 m^3
2.	4	Pure dolomite	Acidizing	Daily oil production 0.5 m^3, daily gas production 15×10^4 m^3
3.	5	Dolomite containing calcium sulfate	Acid fracturing	Cumulative oil production 74.93 m^3, cumulative gas production 2×10^4 m^3
	5	Dolomite containing calcium sulfate	Hydraulic fracturing with proppant	Cumulative gas production 1.4×10^4 m^3
4.	40	Pure dolomite	Acid fracturing	Daily liquid production 36.6 m^3, water-bearing stratum
5.	10	Pure dolomite	Acid fracturing	Daily liquid production 241 m^3, a small amount of gas
6.	5	Mudstone and dolomite	Acid fracturing	The pumping pressure is too high and the acid fracturing is not completed

dolomite would greatly reduce the conductivity. Li developed the hydraulic jet acid fracturing technology to solve the problems of high temperature, high fracture pressure, high friction, and strong heterogeneity faced by the stimulation of deep carbonate rocks (Li et al. 2012). Wang studied the fine segmented design method and developed the high-temperature resistant authigenic acid and gelling acid for ultra-deep carbonate rocks, aiming at the problems of fast reaction between acid and rock, short action distance of acid and low fracture conductivity under high closure stress (Wang et al. 2021). In addition, the use of encapsulated acid is also an important means to achieve high-efficiency treatment of deep carbonate rocks (Luo et al. 2019a, b).

Generally speaking, the primary problems of dolomite reservoir treatment include great acid leak-off caused by the development of natural fractures (Fu et al. 2019), fast acid-rock reaction caused by high reservoir temperature (Rabie et al. 2014; Sayed et al. 2013), difficult maintenance of conductivity in acid-corroded fractures caused by high Young's modulus, large Poisson's ratio, and high crustal stress (Desouky et al. 2020; Mehrjoo et al. 2022), poor conductivity caused by uniform etching of dolomite with high purity (Zhang et al. 2020), difficult vertical effective operation caused by numerous vertical small layers and thick reservoirs, and difficult fracture caused by great fracture pressure gradient of the reservoir (Yan et al. 2021a). Therefore, the corresponding treatment measures were proposed as follows: liquid thickening (Luo et al. 2021), leak-off suppression with solid particles (Pankov et al. 2012), pre-flush fluid cooling (Lei et al. 2018; Zhang et al. 2022), large-displacement treatment (Han et al. 2017), closed acidification (Aljawad et al. 2019), sand-acid fracturing (Zhang et al. 2021), diversion acid fracturing (Rabie et al. 2012), and so on.

However, the ultra-deep subsalt dolomite reservoir in Tarim Basin is significantly different from other dolomite reservoirs, with higher temperatures, higher formation pressures, probable secondary precipitation caused by gypsum, and greater treatment difficulty (Hu et al. 2021; Peng et al. 2018; Yan et al. 2021c). Therefore, it is necessary to propose targeted treatment strategies based on a deep analysis of the reservoir characteristics and treatment difficulties, to form appropriate treatment processes, and optimize treatment parameters, for the efficient development of the ultra-deep subsalt dolomite gas reservoir in Tarim.

Difficulties and measures of reservoir treatment

In the Tarim oilfield, 23 subsalt ultra-deep dolomite wells were exploited, and seven treatment measures were implemented for 6 of these wells. The treatment process included acid fracturing by multi-stage alternating injection, temporary plugging followed by sand fracturing, and acidizing. Three treatment measures were implemented for the dolomite reservoir, and another three measures were implemented for the gypsum-containing dolomite reservoir, with the treatment well depth range majority of about 8000 m, reservoir temperature range of 130–170 °C, displacement range of 2.5–7.1 m^3 min^{-1}, total liquid volume range of 140–1310 m^3, and extension pressure gradient range of 1.83–2.46 MPa/100 m. After the treatment, the output of wells in different formations and different processes varied greatly, and the treatment performance was not satisfactory. The treatment difficulties are the following (Cai et al. 2009; Su et al. 2019; Yang et al. 2020a):

1. Treatment treatment pressure is high. The reservoir is deep, and the fracture pressure gradient and fracture extension pressure gradient are high. Therefore, the treatment is difficult and requires more rigid treatment string and injection equipment.

2. The effective working distance of acid is limited. The reservoir temperature is high in the range of 130–170 °C, and thereby the reactions between acid and reservoir rock are fast. A large proportion of acid is consumed at the fracture opening, and the length of acid-corroded fracture is small.

3. Reservoir fractures and cavities are developed, acid fluid leak-off is obvious during fracturing, and liquid efficiency is low. The leak-off balanced and microfracture leak-off zigzag types are dominant in the gypsum-containing dolomite acid fracturing wells. The etching ability of acid for the fractured wall is limited, and the acid-corroded fracture is narrow, resulting in high net pressure in the fracture; The fracture-height-out-of-control, connected-natural-fracture, and leak-off balanced types are dominant in the acid fracturing dolomite reservoir. The net pressure in the fracture is constant or declines gradually.

4. The effluent is serious after acid fracturing treatment. The buried depths of some wells exceed the oil–water/gas–water interfaces, so water is easy to produce after treatment. In contrast, the gas output of some wells with the same depths exceeds $15 \times 10^4 m^3$ d^{-1} without water production.

5. The adaptability of the acid system is poor. The treatment success rate of gypsum-containing dolomite reservoir is low, and treatment is difficult because the existing treatment liquid or process is not suitable. The gypsum-containing dolomite reservoir is acidified with ordinary gelling acid with a low corrosion rate, leading to the reinforcement of rock plasticity and difficult fracture initiation and propagation; the non-uniform etching of gypsum-containing dolomite is of low efficiency in the presence of the acid, and the corrosion rate, as well as

conductivity of acid-etching fracture, are low, leading to difficult prop at a high closing pressure and rapid decline of output.

Targeting these treatment difficulties, the following treatment countermeasures are proposed:

1. CaCl$_2$ weighted fracturing fluid is selected as the pre-flush fluid for fracturing and opening the reservoir in the early stage, and KCl weighted fracturing fluid is selected in the later stage to improve the hydrostatic pressure of the fluid in the well and to reduce the risk of wellhead overpressure, so the requirements of pipe string and injection equipment will be less stringent. Adding CaCl$_2$ and KCl, the density of fracturing fluid can be increased and the liquid column pressure can be increased, thus avoiding increasing the bottom hole pressure by increasing the wellhead pressure (Mao et al. 2022; Yang et al. 2020b).
2. First, a large amount of pre-flush fluid is injected to reduce the reservoir temperature and to slow down the reactions between acid and reservoir rock.
3. The gel fracturing fluid with high viscosity is selected as the pre-flush fluid to reduce the leak-off of acid. The multi-stage alternating injection process is adopted for the injection course to reduce the leak-off of acid, improve the liquid efficiency, and increase the working distance of acid.
4. On the premise of ensuring the treatment safety and integrity of the whole life cycle of the well, the displacement is gradually increased to prevent the breaking of the reservoir and connection of aquifers.
5. Multi-stage alternating injection and closed acid fracturing treatment process are adopted. Cross-linked acids are preferable, and acids with high and low viscosities are alternately injected to realize the deep etching of near and far well zones. Closed acid fracturing is adopted for near wells to improve the fracture conductivity; In the early stage of acid injection, acid with low viscosity is used for etching to activate the natural fractures around the well.

Optimization of the treatment process

Based on the reservoir characteristics, treatment difficulties, and treatment countermeasures, the treatment process is optimized, and the fracture length and conductivity are optimized.

Treatment process optimization

The output in different treatment processes was simulated by using the dynamic analysis model of volume fracturing horizontal well. The seepage differential equation of single-phase compressible micro-fluid in the bedrock when starting pressure gradient can be expressed as follows (Chen et al. 2019; Ren et al. 2015):

$$\nabla^2 P_m - \chi C_L \nabla P_m - \frac{\phi_m \mu C_m}{K_m} \frac{\partial P_m}{\partial t} - \alpha \left[P_m - P_n \right] = 0 \quad (1)$$

where P_m is the pressure of bedrock pore system, MPa; χ is the starting pressure gradient of bedrock, MPa m^{-1}; C_L represents the compressibility coefficient of fluid, MPa^{-1}; ϕ_m is matrix porosity, dimensionless; μ denotes fluid viscosity, mPa s; C_m represents the comprehensive compressibility coefficient of the matrix, MPa^{-1}; K_m represents the permeability of bedrock, D; α is matrix shape factor, $12/L_m^2$; L_m is matrix rock block size, m; P_n is the pressure of natural fracture system, MPa.

The natural fracture system agreed with the Darcy seepage law. Similarly, the control equation of the natural fracture system can be expressed as follows:

$$\nabla^2 P_n - \frac{\phi_n \mu C_n}{K_n} \frac{\partial P_n}{\partial t} + \frac{\alpha K_m}{K_n} \left[P_m - P_n \right] + \frac{q_n \mu}{K_n} \delta \left(M - M' \right) = 0 \quad (2)$$

where C_n represents the compression coefficient of natural fracture, MPa^{-1}; K_n represents the natural fracture permeability, D; q_n represents the volumetric flow rate of liquid at the source divided by that at the sink per unit natural fracture pore volume, s^{-1}; ϕ_n represents the porosity of natural fracture, dimensionless; $\delta \left(M - M' \right)$ is the delta function, of which the value equals 0 when $M = M'$.

As an independent medium system, the seepage of fluid in hydraulic fracture obeys Darcy's law, so its control equation can be expressed as follows:

$$\nabla^2 P_f - \frac{\phi_f \mu C_f}{K_f} \frac{\partial P_f}{\partial t} + \frac{q_f \mu}{K_f} \delta \left(M - M' \right) = 0 \quad (3)$$

where C_f represents the hydraulic fracture compression coefficient, MPa^{-1}; K_f represents the hydraulic fracture permeability, D; q_f represents the volumetric flow rate of liquid at the source divided by that at the sink per unit hydraulic fracture pore volume, s^{-1}; ϕ_f represents the porosity of natural fracture, dimensionless; P_f represents the pressure of hydraulic fracture system, MPa.

The dimensions in Eqs. (1)–(3) were eliminated by mathematical methods, and a finite-element integral equation was

established by using the weighted residual method. The continuous infinite-freedom-degree solving elements were discretized into finite elements for the solution, and thereby the output under different fracture conditions can be simulated (Ren et al. 2015).

Targeting the maximizing of output, the treatment schemes of the Cambrian dolomite reservoir, including sand fracturing, acid network fracturing, and conventional acid fracturing, were screened (Zhao et al. 2014); The main parameters used are shown in Table 2, the maximum daily and cumulative output values in different processes are shown in Fig. 1.

The maximum daily and cumulative output in different processes varied greatly. The calculation results show that the reservoir treatment with the acid network fracturing technique could activate the natural fractures to the greatest extent to form a complex fracture network (Fig. 2), so the daily and cumulative output could be maximized. Therefore, the acid network fracturing technique is preferable. During treatment, an acid system with low viscosity should be injected to activate the natural fractures around the well in the early stage of injection; Then, different acid systems with low and high viscosities should be alternately injected to realize the deep etching of near and far wells. The alternate injection of high viscosity acid and low viscosity acid

with two purposes: (1) Alternate injection of high and low viscosity acid fluid to form a finger phenomenon, improve the degree of non-uniform etching, and then improve the conductivity; (2) Etching can be realized in the whole injection process, avoiding the defect of low etching efficiency when fracturing fluid is used alternately.

The pressure conditions for the activation and extension of natural fractures were analyzed by using the interaction criterion between artificial and natural fractures (Luo et al. 2018). Warpinski and Teufel proposed the shear slip criterion for intersection interaction perpendicular to natural fractures, and this criterion can be expressed by Eq. (4):

$$|\tau| \geq \tau_0 + \mu_f(\sigma_n - p_{junc}) \tag{4}$$

The intersection pressure p_{junc} is replaced by the net pressure p_{net} in the fracture, and the stress τ and σ_n can be expressed by the far-field stress σ_{hmin} and σ_{Hmax}. The intersection criterion can be expressed as follows:

$$p_{net} \geq \frac{\tau_0 - (\sigma_{H\max} - \sigma_{h\min})(\sin 2\beta + \mu_f \cos 2\beta - \mu_f)/2}{\mu_f} \tag{5}$$

where τ_0 is the shear strength of the natural fracture.

Table 2 Main parameters used in numerical simulation

Item	Value	Item	Value
Reservoir size (m)	500*500*30	Number of natural fractures	10
Matrix permeability (mD)	0.18	Fracture permeability (mD)	2000
Matrix porosity (dimensionless)	2%	Pore fluid pressure (MPa)	142
Maximum horizontal principal stress (MPa)	181	Minimum horizontal principal stress (MPa)	152

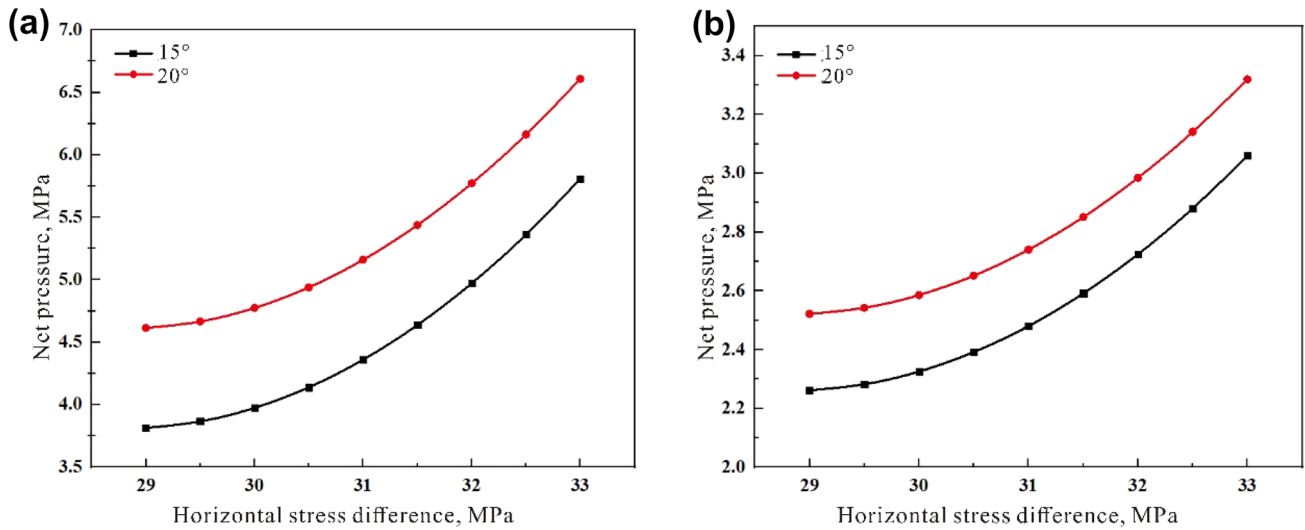Fig.1 Daily and cumulative output in different processes
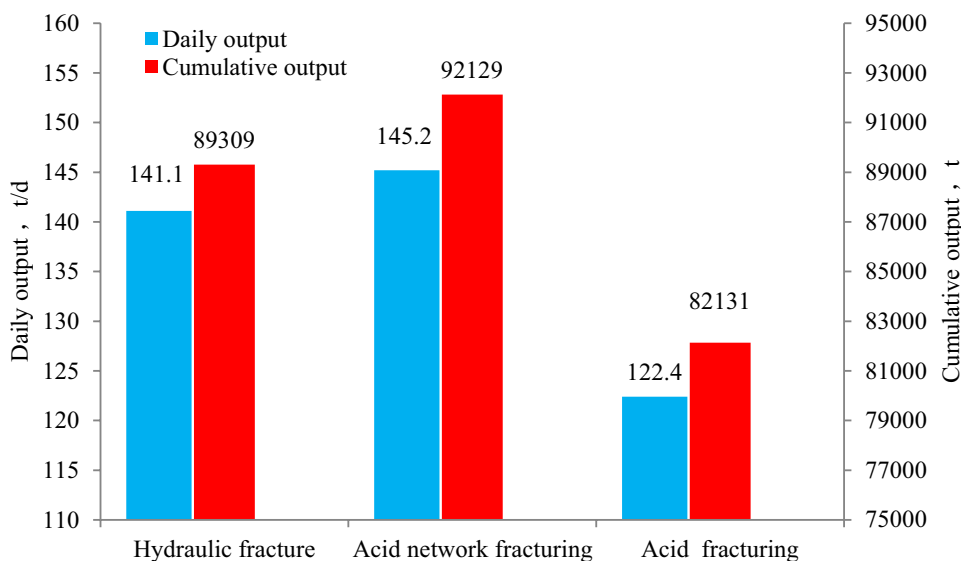
Fig. 2 Pressure conditions of natural fracture activation under different angles between natural fracture and artificial fracture (**a**) and extension (**b**)

Blanton proposed the standard of intersection interaction perpendicular to the closed natural fracture. For the restart of fracture on the other side of the natural fracture, the pressure $p(x_o)$ should be large enough to overcome the stress σ_t parallel to the natural fracture and tensile strength T_o of matrix rock:

$$p(x_o) \geq \sigma_t + T_o = \sigma_{t1} + \sigma_{t2} + T_o \tag{6}$$

The intersection interaction criterion can be expressed in the form of net pressure Pnet:

$$p_{net} \geq p(x_o) + \Delta p_{open} + \Delta p_{shear} - \sigma_{h\min} \tag{7}$$

And,

$$p(x_o) > T_o + \frac{\sigma_{H\max} + \sigma_{h\min}}{2}$$
$$+ \frac{\sigma_{H\max} - \sigma_{h\min}}{2}\left(\cos 2\beta - \frac{v(x_o)}{a}\sin\beta\right) \tag{8}$$

$$v(x_o) = \frac{1}{\pi}\left[(x_o + l)\ln\left(\frac{x_o + l + a}{x_o + l}\right)^2\right.$$
$$\left. + (x_o - l)\ln\left(\frac{x_o - l - a}{x_o - l}\right)^2 + a\ln\left(\frac{x_o + l + a}{x_o - l - a}\right)^2\right] \tag{9}$$

$$x_o = \left(\frac{(1+a)^2 + e^{\frac{\pi}{2\mu_f}}}{1 + e^{\frac{\pi}{2\mu_f}}}\right)^{1/2} \tag{10}$$

where Δp_{open} is the pressure loss in the direction of the length of activated natural fracture l; Δp_{shear} is the pressure loss in the direction of shear natural fracture length a, and x_o represents the distance between the restart and intersection points.

The criterion for the fracture restart at the tip of activated natural fracture can be described as follows:

$$p_{tip} = p_{junc} - \Delta p_{nf} \geq \sigma_E + T_o \tag{11}$$

where p_{tip} is the fluid pressure at the tip of the natural fracture, and Δp_{nf} represents the pressure loss in the direction of the natural fracture.

Similarly, Eq. (11) can be expressed as follows: $p_{net} \geq \frac{1}{2}(\sigma_{H\max} - \sigma_{h\min})(1 - \cos 2\beta) + T_o + \Delta p_{nf}$ (12)

The horizontal stress difference of Wusonger formation in Tarim subsalt dolomite was 29 MPa, and the azimuth angle between natural fracture and principal stress was around 15°; The horizontal stress difference of Shayirik formation was 33 MPa, and the azimuth angle between natural fracture and principal stress was about 20°; The pressure conditions for the activation and extension of natural fractures in Fig. 2 show that the net pressure required to activate natural fracture increased with the increase in the angle and horizontal stress difference. The maximum activated net pressure was almost 7 MPa, and the natural fractures with great stress difference and large angles were difficult to activate; The extension pressure after the opening and activation of natural fractures was in the range of 2–3.5 MPa, at a medium level, indicating that the

activation of natural fracture was vital to the treatment of fracture network. Considering the limited pump pressure during treatment, chemical corrosion with acids could be synergistically combined with mechanical interaction to activate natural fractures. On the one hand, some carbonate fillings can be dissolved through the pretreatment of the acid, on the other hand, the mechanical properties of the reservoir rocks can be reduced, thereby reducing the fluid pressure that activates the natural fracture.

Fracture length

With the preferable technique of acid network fracturing, the output change after single-stage treatment and compaction was simulated. The fracture lengths of single-stage fractures were set to 100, 120, 150, and 180 m, and the effectively closed conductivity was set to 30 D cm. Twenty natural fractures were activated. The daily and cumulative output under the different conditions of fracture lengths was calculated, and the results are shown in Fig. 3.

When the fracture length is 100, 120, 150, and 180 m, respectively, the initial daily output of oil is about 105, 127,147, 163 t d^{-1}, the stable daily output is about 9, 13, 17, 20 t d^{-1}, and the cumulative oil is about 0.64×10^5, 0.8×10^5, 0.93×10^5, 1.04×10^5 t. The increase in cumulative oil is 0.16×10^5, 0.13×10^5, and 0.11×10^5 t, respectively. The longer the fracture was, the larger the treatment range was, and the smaller the seepage resistance was. Therefore, the daily and cumulative output increased. When the effective fracture length exceeded 150 m, the

output increased to a smaller extent. Therefore, the fracture length value of 150 m was preferable.

Conductivity capacity

The conductivity of artificial fractures is another important index for the evaluation of treatment performance, and it affects the production performance after treatment. It is necessary to optimize the conductivity of fracture after the acid network fracturing process. In the simulation and calculations, the length of the single-section fracture was set to be 150 m, twenty natural fractures were activated. The daily and cumulative output under the different conditions of conductivity capacity of 10, 20, 30, and 40 D·m was calculated, and the results are shown in Fig. 4.

When the conductivity is 10, 20, 30, and 40 D cm, the initial daily output of oil is about 90, 123, 147, and 158 t d^{-1}, respectively, and the cumulative oil is 0.66×10^5, 0.8×10^5, 0.93×10^5, and 0.99×10^5 t, respectively, with an increase of 0.14, 0.13, and 0.07 t, respectively. The greater the conductivity capacity was, the smaller the flow resistance was, and the greater the daily and cumulative output were; the cumulative output with conductivity capacity in the range of 30–40 D cm was close to the single-section controlled output; when the conductivity capacity exceeded 30 D cm, the contribution of increased conductivity capacity to the output was weakened. Therefore, the conductivity capacity value of 30 D cm was preferable.
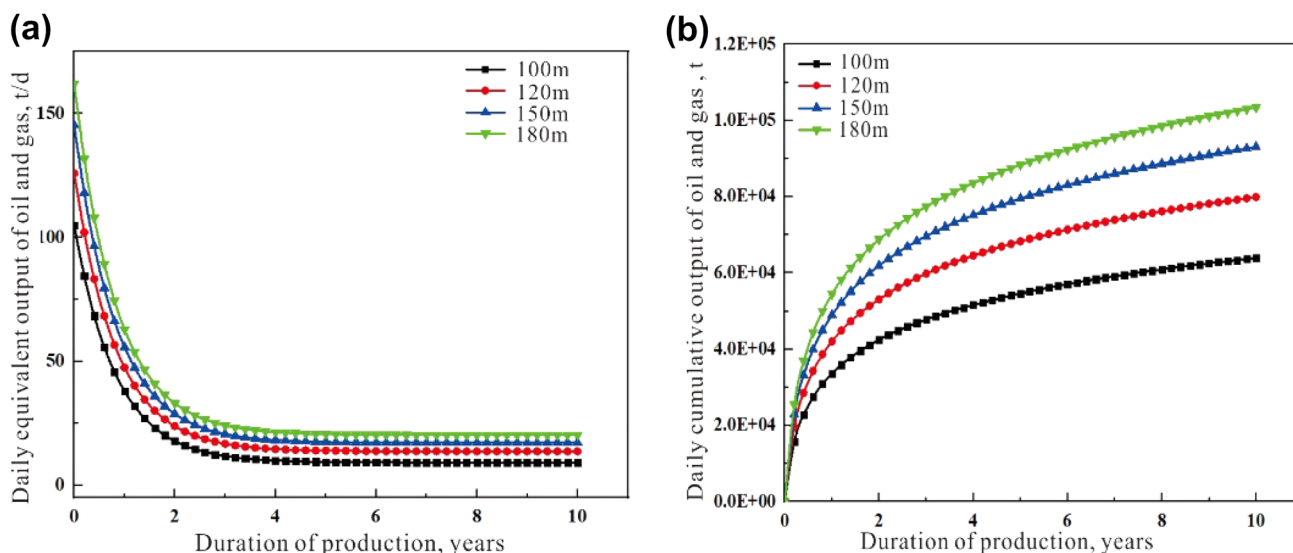

Fig. 3 Daily (**a**) and cumulative (**b**) output under the different half-lengths of fracture

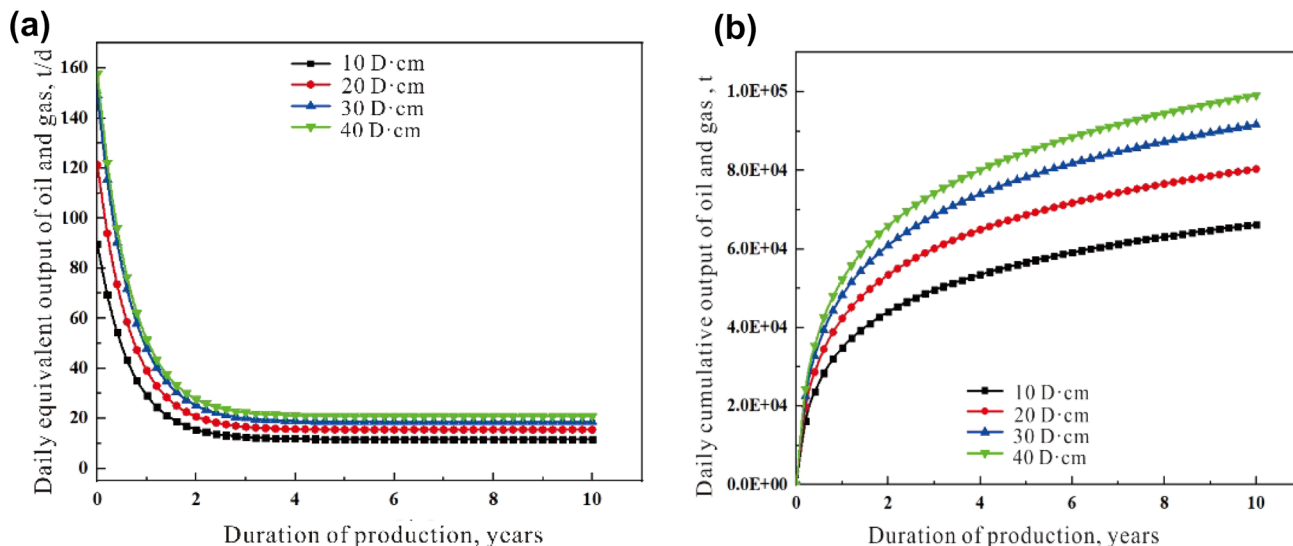**(a)**

(b)

Fig. 4 Daily (**a**) and cumulative (**b**) output under the different conductivity capacity

Evaluation of the performance of acid fracturing materials

According to the optimization results of process parameters, the performances of acid, fracturing fluid, and etching were evaluated separately to judge whether the materials met the treatment requirements.

Fracturing fluid system

For the reduction in wellhead treatment pressure and the harshness of requirements for the performance of injection string and equipment for the dolomite reservoir, the wellbore hydrostatic pressure should be increased (Dai et al. 2019; Liu et al. 2020). Therefore, $CaCl_2$ (first section) and KCl (second and third sections) weighted fracturing fluids were selected for alternate injection.

The viscosity of $CaCl_2$ and KCl weighted fracturing fluids was measured with a Huck MARSIII rotary rheometer with a shear rate of 170 s^{-1} and heating rate of 1 °C min^{-1}. The relationship between sample viscosity and temperature was recorded. The test results are shown in Figs. 5 and 6.

The initial viscosity of $CaCl_2$ weighted fracturing fluid was about 90 mPa s. With the increase in temperature, the viscosity first increased and then declined. 30 min later, the viscosity reached a maximum of about 500 mPa s at about 140 °C. After that, the viscosity gradually declined to about 200 mPa s, and the leak-off of the acid system to natural fractures could be impeded to a large extent. In contrast, the rheological profile of KCl weighted fracturing fluid was different from that of $CaCl_2$ weighted fracturing fluid. The initial viscosity of KCl weighted fracturing fluid was about 950 mPa s. With the increase in temperature, the viscosity
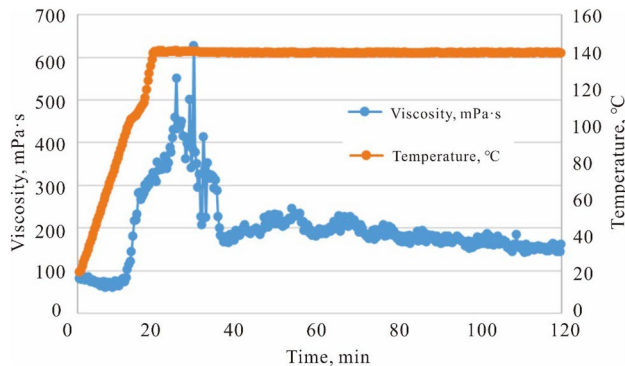

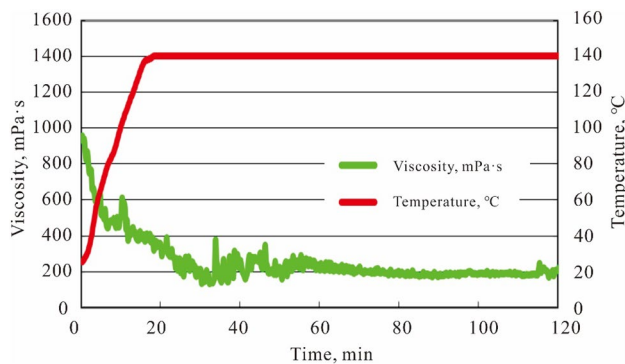**Fig. 5** Rheological profile of $CaCl_2$ weighted fracturing fluid

Fig. 6 Rheological profile of KCl weighted fracturing fluid

gradually declined. 30 min later, the viscosity declined to a value of about 200 mPa s and then was kept constant. According to the rheological characteristics of $CaCl_2$ and

KCl weighted fracturing fluids, the former was selected as the fracturing fluid in the first stage. Its high viscosity suppressed leak-off and promoted the formation of high pressure at the well bottom to open the reservoir and generate fractures; the latter was selected as the fracturing fluid in the form of alternate injection in the following stages to reduce reservoir temperature and acid fluid leak-off.

Acid system

Gelling and retarded acid were the candidates for acid systems. According to the industry standard SY/T 5886-2012 "Evaluation approach of retarded acid performance," the corrosion rate, etching morphology, and conductivity capacity of acid-etching fracture of 20% gelling acid and 20% retarded acid (pH = 4–5) for gypsum-containing dolomite were tested. The results are shown in Table 3.

The corrosion rates of gelling acid and retarded acid for the gypsum-containing dolomite were similar; the corrosion rate of gelling acid was in the range of 44.42−61.34%, and the average corrosion rate was 51.72%; the corrosion rate of retarded acid was in the range of 45.19–55.93%, with a mean value of 50.56%.

Table 3 Corrosion rates with different acids

Acid type	Sample number	Corrosion rate (%)
20% gelling acid	3–22/65	61.34
	4–14/35	49.40
	9–23/73	44.42
	Average corrosion rate	51.72
20% retarded acid	3–22/65	55.93
	4–14/35	45.19
	Average corrosion rate	50.56

The etching for gypsum-containing dolomite was carried out by using 20-min displacement experiments. The etching morphologies of gypsum-containing dolomite with gelling acid and retarded acid are exhibited in Figs. 7 and 8. The former showed poor etching performance for gypsum-containing dolomite, and only local pitting corrosion was observed. The conductivity test was carried out after etching. When the closing pressure was in the range of 5–10 MPa, almost no outflow was observed at the outlet, and high pressure was held at the inlet; In contrast, the rock plate showed a good etching morphology with local etching grooves with retarded acid.

Figure 9 shows the conductivity of the two acid liquids under different closing pressures. With the increase in closure pressure, the conductivity decreases rapidly. However, since retarded acid can form better non-uniform etching than that of gelling acid (Figs. 7 and 8), the conductivity of retarded acid etched fracture is still higher than that of gelling acid. Under the closing pressure of 5 MPa, the conductivity of retarded acid etched fracture is about 9 D cm, while that of gelled acid etched fracture is about 7.5 D cm. Under the closing pressure of 60 MPa, the conductivity of retarded acid etched fracture is about 1.5 D cm, while that of gelled acid etched fracture is about 0.5 D cm.

Field application

Taking well Z2 as an example, the field experiment of acid fracturing technology of ultra-deep dolomite reservoir was performed. Well Z2 was 8791 m deep, and the acid fracturing treatment was carried out in the 8376–8406-m well section, where the reservoir texture was granular and fine-grained dolomite and contained fracture pores mostly semi-filled with calcite and dolomite; This section consisted of 2
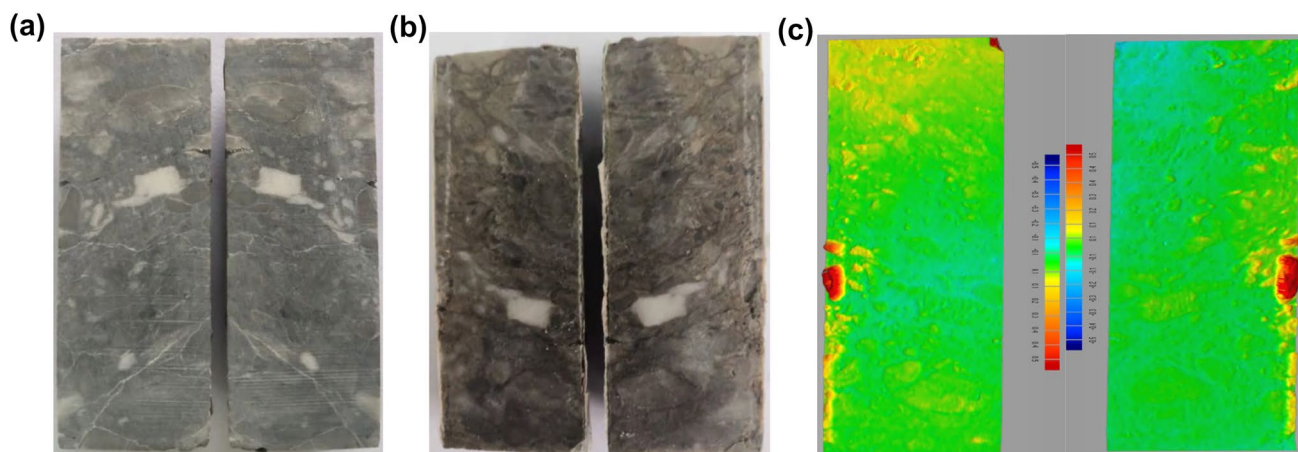

Fig. 7 Morphologies of gypsum-containing dolomite before (**a**) and after (**b**) corrosion with gelling acid and surface scanning image after corrosion (**c**)
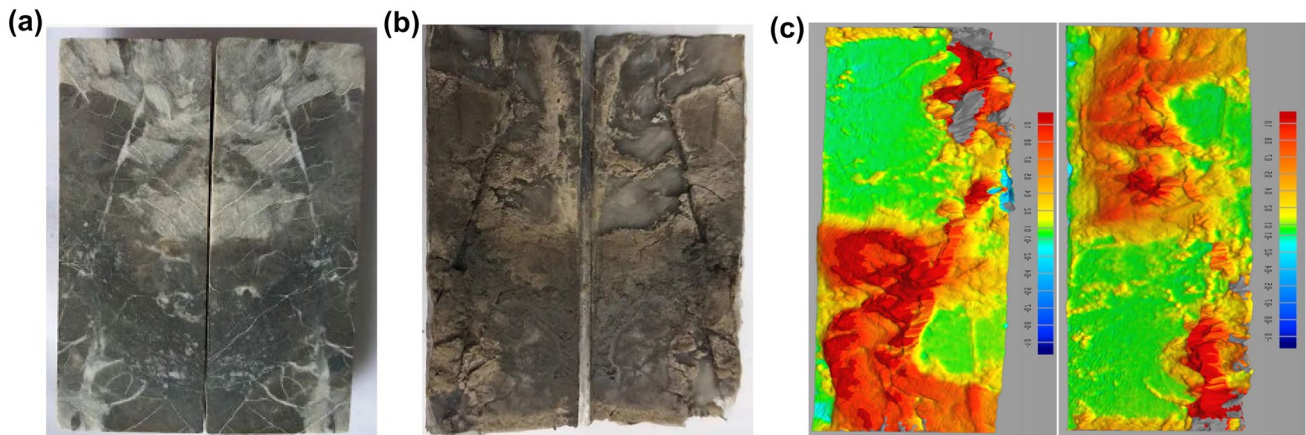
Fig. 8 Morphologies of gypsum-containing dolomite before (**a**) and after (**b**) corrosion with retarded acid and surface scanning image after corrosion (**c**)

layers of the class-II reservoir with a thickness of 6.5 m and porosity of 3–3.2% (mean value is 3.1%) and 6 layers of the class-III reservoir with a thickness of 39.5 m and porosity of 1.3–1.8% (mean value is 1.61%); The well bottom was at about 157 °C; The treatment section was at 8648–8683 m, with high crustal stress. The minimum horizontal principal stress was in the range of 174.9–180.8 MPa, and the horizontal stress difference was in the range of 38.9–44.8 MPa. The brittleness index was greater than 65, and the average compressibility index was 0.5, indicative of high compressibility (Yan et al. 2019); 30 natural fractures were developed in the treatment section, and most of the dip angles of fractures were in the range of 55°–85°, so these fractures were ready to activate.

According to the results of reservoir characteristics, reservoir treatment difficulties and countermeasures, treatment process and fracture parameter optimization, and acid fracturing material performance evaluation, the injection procedure was designed and is shown in Table 4.
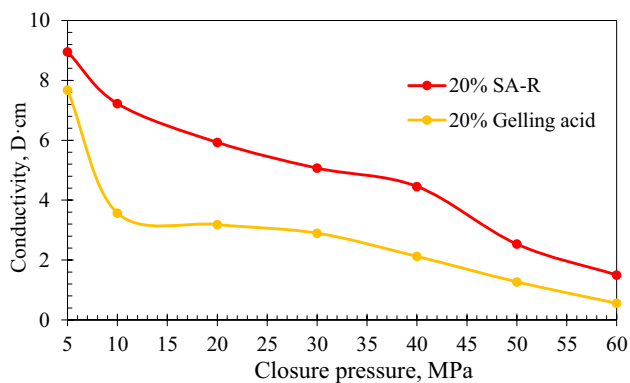

Fig. 9 Conductivity of two acid liquids under different closure pressures

According to the pumping procedure shown in Table 4, the field implementation was carried out. The treatment profile is shown in Fig. 10. The injection commenced at 17:45, and the pressure and displacement gradually increased. At 18:7, under the condition of constant displacement, the oil pressure continued to decrease, confirming that the fracture was opened and the fracture was extended normally. Before the decrease in oil pressure, the maximum oil pressure reached 113 MPa, and the well bottom pressure was evaluated to be about 180.4 MPa; At 18:35, the displacement increased and oil pressure increased accordingly. In the subsequent injection process, the decrease in oil pressure was observed many times under the condition of constant displacement, indicating that multiple natural fractures were connected.

Based on the data of pressure and displacement injected during the treatment, the net pressure fit was conducted, and the geometry of the fracture was simulated through inversion. The simulated fracture was 145 m half-length and 49 m high, which are close to the values (140 and 55 m, respectively) required in the acid fracturing design. Therefore, the treatment was carried out smoothly and successfully.

As shown in Fig. 11, before the acid fracturing treatment (April 2, 2022), a 4-mm nozzle was used for the drainage of well Z2. The oil and casing pressures were 0 and 19.012–18.697 MPa, with a total drainage volume of 0.2 m^3 and without natural gas; The acid fracturing treatment was carried out on April 3. After the treatment, the 4 mm nozzle was still used. The oil pressure was in the range of 18.524–19.613 MPa, equivalent to about 6000 m^3 of gas output per day, indicative of good treatment performance.

Table 4 Acid fracturing injection procedure of well Z2

No.	Treatment step	Liquid volume (m³)	Oil pressure (MPa)	Displacement (m³ min⁻¹)	Note
1.	KCl weighted fracturing base fluid	50	40–100	0–2.5	Small-test fracturing
2.	CaCl₂ weighted fracturing gel fluid	55	99–106	2.0–2.5	Fracturing reservoir
3.	KCl weighted fracturing gel fluid	70	106–112	2.0–2.5	Cooling down and fracturing
4.	Cross-linked acid	120	106–112	2.0–2.5	Acid fracturing with two-stage alternate injection; below the pressure threshold, increasing the displacement as much as possible
5.	KCl weighted fracturing gel fluid	70	106–112	2.0–2.5	
6.	Cross-linked acid	100	106–112	2.0–2.5	
7.	Non-cross-linked acid	60	106–112	2.0–2.5	Closed acidizing to improve the conductivity of near-well zone
8.	Displacement fluid injection with a low displacement	53	95–98	1.0–1.5	Complete displacement with the acid in the reservoir
9.	Stop the pump and measure the pressure drop for 30–60 min				
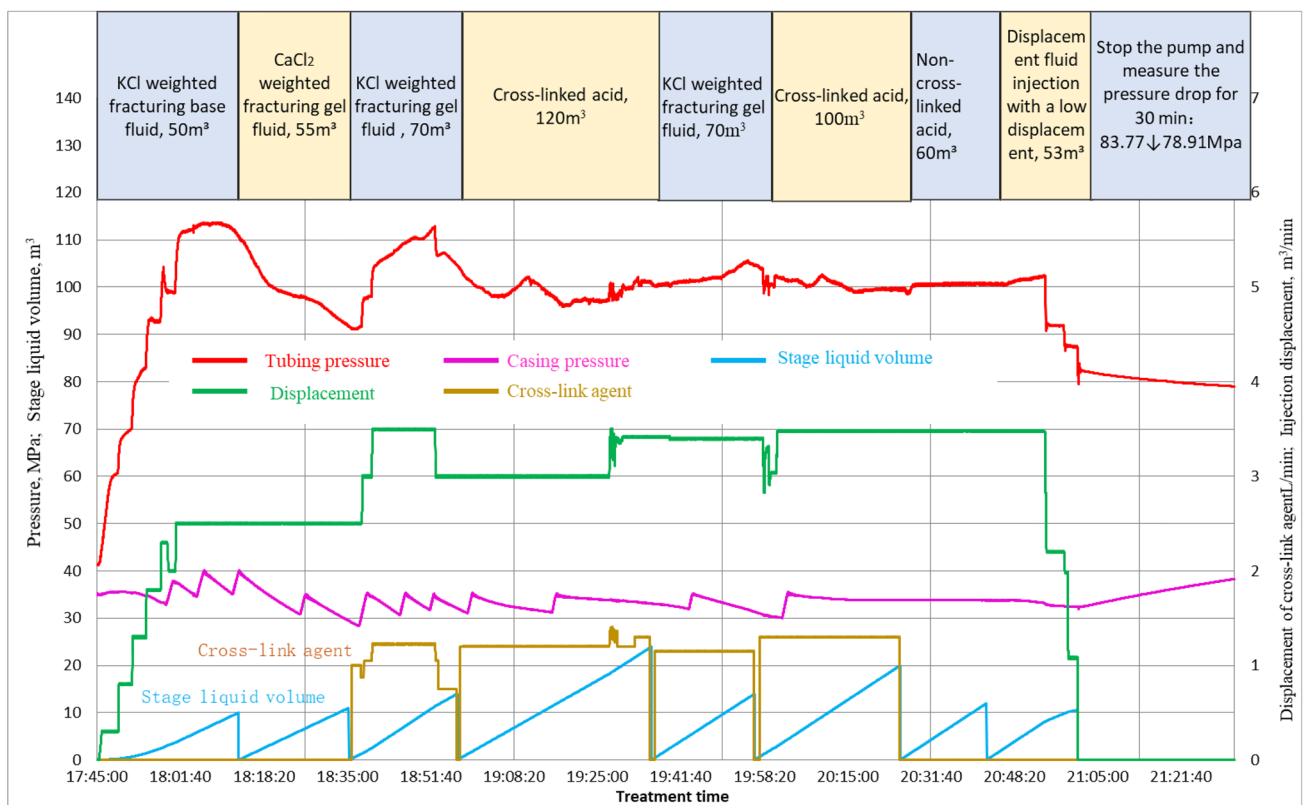
Fig. 10 Pressure profile during treatment injection and displacement injected

Conclusion

The problems of high pressures in the treatment process, a limited effective etching distance of acid, great acid leak-off, and poor adaptability of the acid system are encountered in deep and ultra-deep carbonate reservoirs. The mechanism of acid fracturing stimulation under different processes and parameters is not clear. Based on analyzing the difficulties of dolomite reservoir treatment and the mechanism of different stimulation methods, the corresponding optimal stimulation method is proposed, the mathematical model of ultra-deep reservoir productivity is established, and the optimization design of injecting
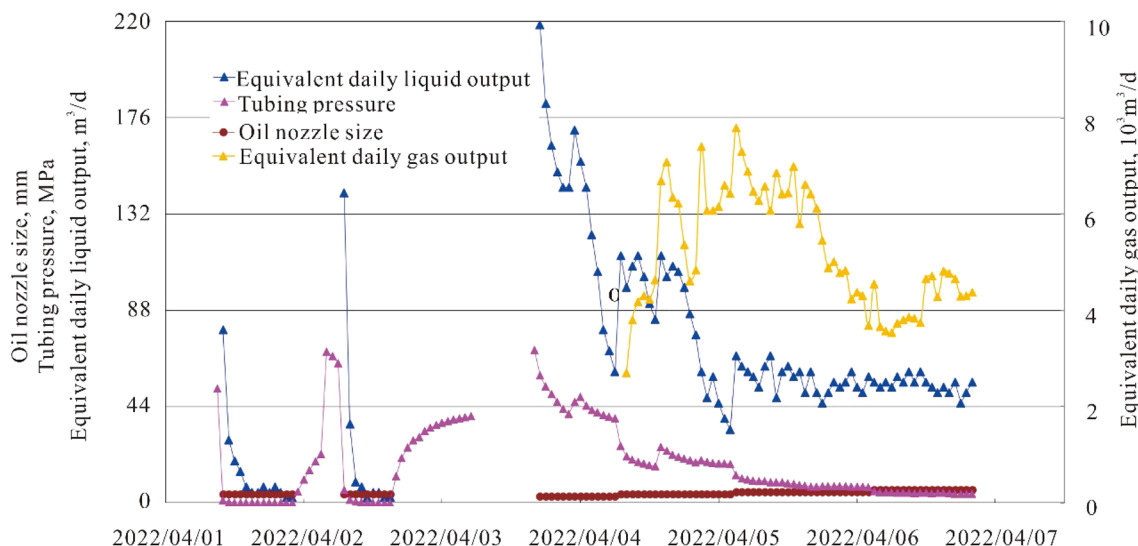
Fig. 11 Output profile of well Z2

process, parameters, and acid fracturing materials is carried out, the following conclusions are obtained:

1. The stimulation mechanism under different treatment methods, injection parameters, and acid fracturing materials is analyzed through numerical simulation and experimental tests, which provides a theoretical basis for the on-site implementation of acid fracturing of the dolomite reservoir.
2. The application of weighted fracturing fluid, pre-flush fluid cooling, leak-off reduction in high-viscosity fracturing fluid, and optimization of treatment processes are crucial to acid fracturing treatment.
3. The application of weighted fracturing fluid could effectively reduce the wellhead pressure, and reduce the harshness of equipment performance required.
4. By using 20% gelling acid and retarded acid, non-uniform etching could be realized to improve the effective action distance of acid and effective conductivity.

Declarations

References

Aljawad MS, Zhu D, Hill AD (2019) Modeling Study of temperature and fracture-propagation effects on the fracture-surface dissolution patterns and fractured-well productivity in acid fracturing. SPE Prod Oper 34:749–769

Cai C, Li K, Li B, Cai L, Jiang L (2009) Geochemical characteristics and origins of fracture- and vug-fillings of the Ordovician in Tahe oilfield, Tarim Basin. Acta Petrol Sin 25:2399–2404

Chen X, Tang C, Du Z, Tang L, Wei J, Ma X (2019) Numerical simulation on multi-stage fractured horizontal wells in shale gas reservoirs based on the finite volume method. Nat Gas Ind B 6:347–356

Dai X, Liu T, Wei J, Wang M (2019) Synthesis and performance of a polymeric thickening agent for weighted fracturing fluids. Drill Fluid Complet Fluid 36:766–770

Desouky M, Tariq Z, Aljawad MS, Alhoori H, Mahmoud M, AlShehri D (2020) Data-driven acid fracture conductivity correlations honoring different mineralogy and etching patterns. ACS Omega 5:16919–16931

Dong R, Wheeler MF, Su H, Ma K (2021) Modeling acid fracturing treatments in heterogeneous carbonate reservoirs. In: SPE international conference on oilfield chemistry, Day 1 Mon, 06 Dec 2021. SPE-204304-MS

Fu S, Zhang C, Chen H, Chen A, Zhao J, Su Z, Yang S, Wang G, Mi W (2019) Characteristics, formation and evolution of pre-salt dolomite reservoirs in the fifth member of the Ordovician Majiagou Formation, mid-east Ordos Basin, NW China. Pet Explor Dev 46:1153–1164

Han X, Yi X-Y, Lu Y, Li Q (2017) Optimum acid-fracturing treatments for ultradeep limy dolomite reservoirs based on conductivity tests. Chem Technol Fuels Oils 53:107–122

Hu W, Wang Q, Zhao R, Ru Z (2021) Evaluation and application of conductivity of strike slip faults in China Shunbei reservoir, Tarim Bacin. Arab J Geosci 14:619

Lei Z, Hu W, Xu H, Xu B, Cao C, Cheng C, Zhu Q (2018) Characteristics of hydrothermal-structure-controlled fracture-vug dolomite reservoir and its influence on oil-water distribution: Lower Cretaceous, Baiyinchagan sag, Erlian Basin, North China. Russ Geol Geophys 59:405–418

Li G, Sheng M, Tian S, Huang Z, Li Y, Yuan X (2012) Multistage hydraulic jet acid fracturing technique for horizontal wells. Pet Explor Dev 39:107–112

Liu Y, Liu J, Li Y, Yang H, Yan F, Zheng J, Wu J, Huang J, Wu Z, Luo C, Lu J (2020) Development and field application of a new ultralow guar gum concentration weighted fracturing fluid in HPHT reservoirs. J Chem. https://doi.org/10.1155/2020/7846372

Luo Z, Zhang N, Zhao L, Yuan X, Zhang Y (2018) A novel stimulation strategy for developing tight fractured gas reservoir. Petroleum 4:215–222

Luo Z, Zhang N, Zhao L, Liu H, Luo P, Liu J (2019a) Innovative encapsulating acid with release dually controlled by the concentration of hydrogen ions and temperature. Energy Fuels 33:4976–4985

Luo Z, Zhang N, Zhao L, Wu L, Liu P, Ren D, Qing C (2019b) A reservoir-damage-free encapsulated acid dually controlled by hydrogen ion concentration and temperature. RSC Adv 9:33733–33746

Luo Z, Cheng L, Zhao L, Xie Y (2021) Study on the mechanism of reactive acid transport in fractured two-mineral carbonate rocks. J Nat Gas Sci Eng 94:104118

Mao J, Liao Z, Jiang J, Yang X, Zhang Y, Tang Y, Liu P, Zhang H, Xue J, Mao J, Lin C (2022) One practical $CaCl_2$-weighted fracturing fluid for high-temperature and high-pressure reservoir. Pet Sci Technol 2022:1–13

Mehrjoo H, Norouzi-Apourvari S, Jalalifar H, Shajari M (2022) Experimental study and modeling of final fracture conductivity during acid fracturing. J Petrol Sci Eng 208:109192

Nino-Penaloza A, Al-Momin A, Zhu D, Hill AD (2015) New insights about acid fracture conductivity at laboratory scale. In: SPE annual technical conference and exhibition. Day 2 Tue, 29 Sept 2015. SPE-174990-MS

Pankov SY, Mukhutdinov RA, Haidar AM, Gorin AN, Baykova VG (2012) Advanced technologies for development and oil reserves involvement of low-permeability dolomite reservoirs in Eastern Siberia. Neftyanoe Khozyaistvo 11:48–51

Peng J, Wang X, Han H, Yin S, Xia Q, Li B (2018) Simulation for the dissolution mechanism of Cambrian carbonate rocks in Tarim Basin, NW China. Petrol Explor Dev 45:431–441

Qi N, Chen G, Pan L, Cui M, Guo T, Yan J, Liang C (2021) Numerical simulation and analysis of fracture etching morphology during acid fracturing of dolomite reservoirs. Chem Eng Sci 229:116028

Rabie AI, Gomaa AM, Nasr-El-Din HA (2012) HCl/formic in-situ-gelled acids as diverting agents for carbonate acidizing. SPE Prod Oper 27:170–184

Rabie AI, Shedd DC, Nasr-El-Din HA (2014) Measuring the reaction rate of lactic acid with calcite and dolomite by use of the rotating-disk apparatus. SPE J 19:1192–1202

Ren L, Su Y, Hao Y, Zhang Q, Meng F, Sheng G (2015) Dynamic analysis of SRV-fractured horizontal wells in tight oil reservoirs based on stimulated patterns. Acta Petrol Sin 36:1272–1279

Sayed MA, Nasr-El-Din HA, Nasrabadi H (2013) Reaction of emulsified acids with dolomite. J Can Pet Technol 52:164–175

Su X, Lian Z, Xiong H, Yuan Y, Fang J (2019) Laboratory study on a new composite plugging material with high bearing strength and high-temperature resistance. J Chem 2019:1874617

Wang Y, Fan Y, Zhou C, Luo Z, Chen W, He T, Fang H, Fu Y (2021) Research and application of segmented acid fracturing by temporary plugging in ultradeep carbonate reservoirs. ACS Omega 6:28620–28629

Yan L, He C, Hou K (2019) A calculation method for brittleness index of shale gas reservoirs based on the imaging spectroscopy mineral maps: a case study of the Lower Silurian Longmaxi shale gas reservoir in the southern Sichuan Basin. Nat Gas Ind 39:54–60

Yan F, Shi Y, Tian Y (2021a) Synthesis and characterization of surfactant for retarding acid–rock reaction rate in acid fracturing. Front Chem 9:715009

Yan L, Liu Q, Liu X (2021c) Research on damage mechanism of ordovician carbonate reservoir in Halahatang Oilfield, Tarim Basin. Fresenius Environ Bull 30:4591–4599

Yan J, Cui M, He A, Qi N, Cui W, Wen X (2021b) Study on boundary of control models and mechanisms of acid rock reaction in carbonate reservoirs with different dolomite mass fraction. In: International petroleum technology conference. Day 2 Wed, 24 Mar 2021b

Yang H, Wu G, Scarselli N, Sun C, Qing H, Han J, Zhang G (2020a) Characterization of reservoirs, fluids, and productions from the Ordovician carbonate condensate field in the Tarim Basin, northwestern China. AAPG Bull 104:1567–1592

Yang X, Mao J, Zhang W, Zhang H, Zhang Y, Zhang C, Ouyang D, Chen Q, Lin C, Zhao J (2020b) Tertiary cross-linked and weighted fracturing fluid enables fracture stimulations in ultra high pressure and temperature reservoir. Fuel 268:117222

Zhang H, Zhong Y, Zhang J, Zhang Y, Kuang J, Yang B (2020) Experimental research on deterioration of mechanical properties of carbonate rocks under acidified conditions. J Petrol Sci Eng 185:106612

Zhang N, Luo Z, Chen X, Zhao L, Zeng X, Zhao M (2021) Investigation of the artificial fracture conductivity of volcanic rocks from Permian igneous in the Sichuan Basin, China, with different stimulation method using an experiment approach. J Nat Gas Sci Eng 95:104234

Zhang N, Luo Z, Zhao L, Zhu R, Chen W, Liu G, Chen X, Xie Y, Cheng L (2022) Innovative thermo-responsive in-situ generated proppant: laboratory tests and field application. J Petrol Sci Eng 208:109514

Zhao Y, Zhang L, Luo J, Zhang B (2014) Performance of fractured horizontal well with stimulated reservoir volume in unconventional gas reservoir. J Hydrol 512:447–456